J. Fluid Mech. (1996), vol. 321, pp. 371 393

Shear-induced radial segregation in bidisperse suspensions

By GOKUL P. KRISHNAN†, SHANNON BEIMFOHR AND DAVID T. LEIGHTON‡

Department of Chemical Engineering, University of Notre Dame, Notre Dame, IN 46556, USA

(Received 12 October 1995 and in revised form 11 April 1996)

In this paper, we discuss experimental evidence for radial particle segregation in a parallel-plate geometry. The motion of coloured tracer particles of a size different from the bulk suspension is followed as a function of time. The tracer particles are seen to experience a constant drift velocity independent of their radial position. This is in addition to the random-walk motion arising from their interactions with other particles in the suspension. These observations are found to be consistent with the shear-induced migration model of Leighton & Acrivos (1987 *a,b*) as well as the tracer diffusivity measurements of Phan & Leighton (1996). In the experiments of Abbott *et al.* (1991), it was observed that larger particles migrated radially outward to regions of lower shear stress in a wide-gap Couette device. In our experiments large tracers were also observed to migrate radially outward. In this case, however, the radial migration resulted in migration to regions of higher shear stress, contrary to expectations. This apparent discrepancy is explained in terms of a model that incorporates both the stress-induced migration of earlier studies and a curvature-induced migration flux (which in turn is shear-induced) as an opposing effect.

1. Introduction

Recent studies have led to at least a partial understanding of the shear-induced migration of particles across streamlines in monodisperse suspensions of non-colloidal particles at low Reynolds number. Geometries which have been studied include tube (Chapman 1990) and channel (Koh, Hookham & Leal 1994; Leighton & Acrivos 1987*b*) Poiseuille flow, wide-gap Couette flow (Abbott *et al.* 1991), Couette reservoir flow (Leighton & Acrivos 1987*b*; Chow *et al.* 1994), resuspension flow (Leighton & Acrivos 1986; Chapman & Leighton 1991; Schaflinger, Acrivos & Zhang 1990) and parallel-plate flow (Chapman 1990; Chow *et al.* 1994). In general, particles are found to preferentially concentrate in regions of lower shear stress and/or lower curvature. Some of the same flows which lead to steady-state non-uniformities in concentration profiles in monodisperse suspensions have also been demonstrated to cause segregation by particle size in bidisperse suspensions. The degree of segregation by size is typically much greater than the total solids concentration gradient.

In their experiments with suspensions of non-colloidal particles in a wide-gap Couette device, Abbott *et al.* (1991), found a preferential migration of the particles

† Current address: Lucent Technologies, Bell Laboratories Innovations, Room 2E27, 2000 N.E. Expressway, Norcross, GA 30071, USA.

‡ Author to whom correspondence should be addressed.

towards the outer wall which was attributed to migration towards regions of lower shear stress. Experiments with bidisperse suspensions demonstrated almost complete size segregation with larger particles forming close packed layers at the outer wall. The particle migration and size segregation was explained in terms of the shear-induced migration mechanisms resulting from a flux of particles down gradients in shear stress.

In this paper, we discuss experimental evidence for particle size segregation in the parallel-plate geometry. The behaviour of tracer particles in a 45% solids volume fraction suspension of non-colloidal spheres sheared in a parallel-plate viscometer at low Reynolds number was investigated. The tracer particles were seen to migrate radially, with the tracer particles larger than those making up the suspension migrating radially outward and those smaller than the average size migrating inward. While this is superficially similar to the results of Abbott *et al.*, in this case the large particles were migrating to regions of higher shear stress. The particle migration and segregation described here are interpreted in terms of the curvature of the flow geometry.

In the next section, we will develop a simple theoretical model to describe the shear-induced migration mechanisms that govern the motion of tracer particles in a concentrated suspension. Section 3 describes our experimental apparatus and procedure and §4 describes our results. The final section contains our conclusions and a comparison of our observations to those of Abbott *et al.* (1991).

2. Theory

The behaviour of monodisperse suspensions in different flow geometries has received much attention in recent years. Notably, Leighton & Acrivos (1987*b*) described the migration of particles in a narrow-gap Couette device resulting in a non-uniform concentration profile. It was found that upon initial shearing of a concentrated suspension in the Couette device, the viscosity showed a short-term increase followed by a long-term decay to a steady-state value. The short-term viscosity increase was interpreted as a result of the initial loading procedure during which the suspension was essentially undergoing a channel flow in the Couette gap. Initial shearing of the gap containing such a suspension caused the inhomogeneous concentration profile to relax to a more homogeneous one due to particles migrating across the streamlines. This relaxation was associated with a short-term increase in the relative viscosity. Subsequent shearing, however, led to particle migration from the sheared gap region into the unsheared reservoir and an associated decrease in the apparent viscosity. Both these migration phenomena were described by Leighton & Acrivos (1987*b*) in terms of a diffusive mechanism arising from irreversible particle interactions under the influence of an external flow and were characterized by a shear-induced diffusivity D. Two possible directions of migration were identified: one in the plane of shear, characterized by $D_{\|}$ and another perpendicular to it, characterized by $D_{\perp}$. These shear-induced diffusivities were shown to scale as $\dot{\gamma}a_s^2$ (where $\dot{\gamma}$ is the average shear rate and a_s is the size of the suspending spheres) and their magnitudes were estimated based both on experimental observations and on a qualitative analysis of particle interactions. The crux of the argument proceeds as follows.

To begin, let us consider a test sphere present in an initially inhomogeneous suspension. When the suspension is subjected to an external shear flow the test particle interacts with other surrounding particles. Under purely creeping flow conditions, two smooth interacting spheres never actually touch each other owing to the lubrication singularity at contact. In reality however, surface roughness or irreversible forces

influence the interaction and an interacting particle will be displaced from its original streamline. The direction of the migration averaged over many interactions is dependent on the local suspension properties. A concentration gradient in the vicinity of the test particle would, for example, cause the particle to experience a larger rate of interactions on one side than on the other, resulting in a net migration down a concentration gradient. On the other hand, a region of higher concentration has a higher viscosity and hence a lower local shear rate (under a constant imposed shear stress). Again, owing to a differential in the rate of interactions, this results in an opposing flux of particles from regions of higher shear rate (or lower concentration) to regions of lower shear rate (or higher concentration). Based on the above arguments, as well as kinetic-theory type formulations, a number of constitutive equations have been proposed for concentrated suspensions, e.g. Phillips *et al.* (1992), Leighton & Acrivos (1987*b*), Nott & Brady (1994). It is important to note that in all these models, variations in the size of the interacting particles are not accounted for. In this work, owing to the complexity of multi-particle interactions between unequal sized spheres, we will adopt the model of Leighton & Acrivos, and extend it to describe the behaviour of bidisperse suspensions.

For monodisperse suspensions, Leighton & Acrivos provided expressions for the shear-induced diffusivity of particles both in the plane of shear as well as perpendicular to it. In either case, the diffusivity at high concentrations was expected to scale as

$$D \approx K \frac{\phi_s^2}{\mu} \frac{\mathrm{d}\mu}{\mathrm{d}\phi} \dot{\gamma} a_s^2 \tag{1}$$

where μ is the local viscosity of the suspension, $\dot{\gamma}$ the local shear rate, ϕ_s the local suspension concentration and a_s the radius of the suspending spheres. Here, K is an $O(1)$ quantity dependent on the nature of particle interactions and expected to be different in the plane of shear and perpendicular to it.

Likewise, the flux N_σ induced by a gradient in the shear stress σ (or shear rate) at a uniform concentration was modelled by

$$N_\sigma = -K_\sigma \frac{\phi_s^2}{|\sigma|} \nabla |\sigma| \dot{\gamma} a_s^2 \tag{2}$$

where K_σ is, as is the case for the diffusivity, a weak $O(1)$ function of concentration which depends on the geometry of the shear flow. Typically, it has been found to have a value of about 0.6 in a direction parallel to the plane of shear (Leighton & Acrivos 1987*b*). It has not yet been measured for shear gradients perpendicular to the plane of shear.

If we consider a monodisperse suspension confined in a parallel-plate viscometer, then, from the above arguments as well as those of Phillips *et al.* (1992), we would expect that particles should migrate down gradients in shear stress. Since, in a parallel-plate device, the shear stress is a maximum at the outer edge and zero at the centre, particles would migrate towards the centre of the device resulting in an accumulation of particles at the centre. Such a migration would then produce a decrease of the average shear-stress in the device. Chapman (1990) however, found that the shear-stress in a parallel plate device exhibited no significant variation over a time scale longer than that associated with a shear-induced migration process. Chapman also measured the radial concentration profile of a sheared suspension of 500–600μm PMMA spheres suspended in castor oil, by examining the height of the settled bed which eventually formed after shearing was stopped. No significant radial variation in the concentration profile was observed (see figure 1). Further, more recent experiments involving NMR imaging of 50% concentration suspensions of

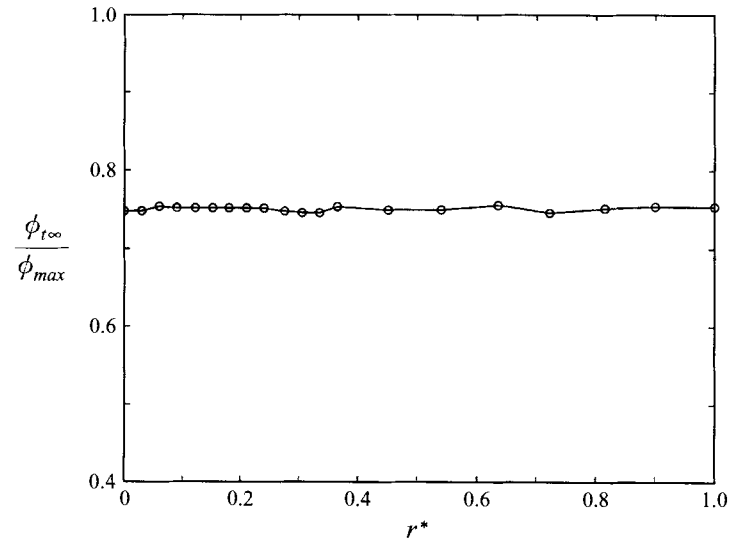

FIGURE 1. Radial concentration profile measurement of Chapman (1990) in a parallel-plate device showing no radial inhomogeneity for a monodisperse suspension.

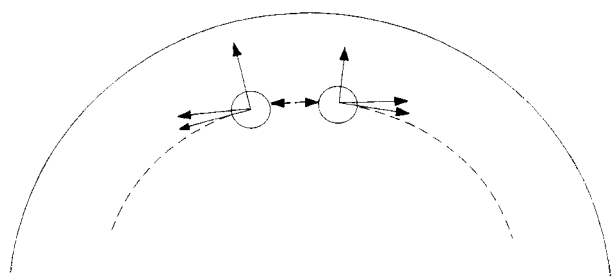

FIGURE 2. Schematic of the interaction between two particles in a curved geometry. An irreversible repulsive force (such as one arising due to the presence of surface roughnesses on the particles) has two components, one acting radially outward and the other tangentially along the line of centres.

monodisperse PMMA spheres in a multi-component fluid of Ucon oil, Triton X-100 and tetrabromoethane in the same geometry conducted by Chow *et al.* (1994) also found no detectable change in the radial concentration profile. These results lead us to believe that there exists some other mechanism of particle migration that counters that due to gradients in shear stress, ultimately resulting in a nearly uniform radial concentration profile for a monodisperse suspension in a parallel-plate device.

One possibility is that in curved geometries such as a wide-gap Couette device or a parallel-plate device there is an additional flux that is induced by the curvature of the shear flow. To understand the origin of this curvature-induced migration better, let us consider the simple schematic shown in figure 2. Suppose we have two equal-sized, suspended particles interacting with each other in the presence of a shear flow. From the observations of previous workers (Arp & Mason 1977; Leighton & Rampall 1993), we know that the presence of surface roughness on the particles acts as a repulsive force tending to keep the two particles apart on the approach (or compression side) of the interaction. This force is in addition to purely hydrodynamic forces, and (unlike hydrodynamic forces under creeping flow conditions) is irreversible – it is present only

during the compression phase of the interaction. Therefore, in a curved geometry we may visualize a force acting on each of the two particles along a line joining their centres. Such a force has two components: one acting along a direction tangential to the local streamwise direction and one acting radially outward. Once the interaction is complete, the two particles get pulled apart as a result of the local shear flow. In this phase of the interaction (or the recession region), the contact force vanishes. As a consequence, the direct result of an irreversible repulsive force is to lead to a radially outward migration in a curved-streamline shear flow. Dimensional arguments analogous to those leading to migration from gradients in shear stress suggest that this flux should scale as $\phi_s^2 \dot{\gamma} a_s^2 / r$ where r is the local radius of curvature of the streamlines.

Based on these simple arguments, we may now combine the flux of particles in a parallel-plate device due to gradients in curvature, shear rate and concentration to yield

$$N_r = K_{r_\perp} \dot{\gamma} a_s \phi_s^2 \frac{a_s}{r} - K_{\sigma_\perp} \phi_s^2 a_s^2 \frac{\mathrm{d}\dot{\gamma}}{\mathrm{d}r} - \hat{D}_\perp \dot{\gamma} a_s^2 \frac{\partial \phi_s}{\partial r} \tag{3}$$

where a_s/r is the dimensionless local curvature of the velocity flow field and $K_{r_\perp}$ and $K_{\sigma_\perp}$ are $O(1)$ constants governing migration in the direction normal to the plane of shear. The quantity $\hat{D}_\perp$ is the dimensionless effective diffusivity normal to the plane of shear (Leighton & Acrivos 1987*b*) which, at steady state, balances the curvature and shear gradient terms. Note that since the gradient in shear rate in a parallel-plate geometry is also given by $\dot{\gamma}/r \equiv \Omega/h$, the two fluxes (due to curvature and shear rate) may be combined as above resulting in a total flux that is independent of radial position:

$$N_r = (K_{r_\perp} - K_{\sigma_\perp}) \frac{\Omega}{h} a_s^2 \phi_s^2 - \hat{D}_\perp \dot{\gamma} a_s^2 \frac{\partial \phi_s}{\partial r}. \tag{4}$$

From the observations that no concentration profile develops in parallel-plate flow for monodisperse suspensions, it is apparent that in this case the two mechanisms largely cancel out ($K_{r_\perp} - K_{\sigma_\perp} \approx 0$). Note that it is not necessary for these effects to exactly cancel out. Rather, the net radial flux is simply sufficiently small that, when balanced at steady state by the diffusive flux, the resulting concentration gradient is smaller than could be measured by Chapman (1990) or Chow *et al.* (1994).

The description for particle migration provided thus far was developed for monodisperse suspensions. In order to extend this to bidisperse suspensions, let us first examine the motion of tracer particles of the same size as those making up the suspension, e.g. $a_t/a_s = 1$. This is the situation, for example, in which a small number of the suspension particles are simply labelled in some way. For this situation, we have the tracer particle flux $(N_r)_t$ by analogy to equation (3) as

$$(N_r)_t|_{a_t/a_s=1} = \frac{\phi_t}{\phi_s}(N_r)_s - \hat{D}_\perp^{tr} \dot{\gamma} a_s^2 \phi_s \frac{\partial(\phi_t/\phi_s)}{\partial r} \tag{5}$$

where $(N_r)_s$ is the total particle flux, ϕ_t is the concentration of the tracers and ϕ_s is the overall suspension concentration (e.g. that of the unlabelled spheres provided $\phi_t \ll \phi_s$). The tracer flux is seen to be composed of two terms, the first of which is just the fraction of the total particle flux corresponding to the tracers. The origin of the second term is more complex. It is possible to envisage a situation in which the tracer particles are *not* distributed uniformly relative to the other particles in the suspension, for example if particles are labelled only in one region. In this case, the tracer flux will have an additional term arising from the random motion of the tracer particles as the suspension is sheared. This random walk motion is characterized by

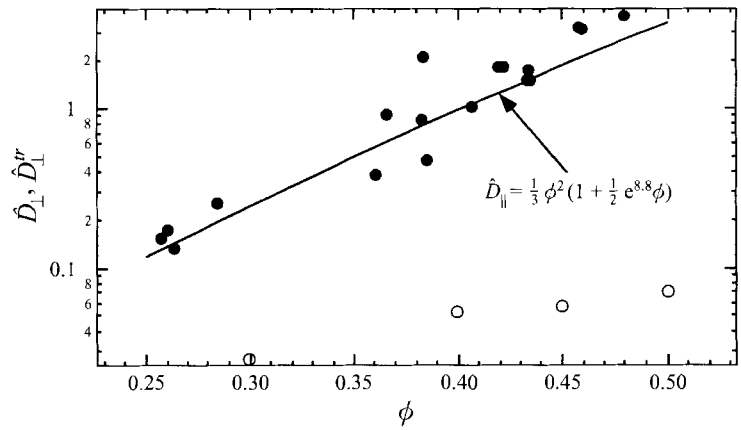

FIGURE 3. Comparison of the effective diffusivity, $\hat{D}_\perp$ (•) with the tracer diffusivity normal to the plane of shear, $\hat{D}_\perp^{tr}$ (○), shows the latter to be an order of magnitude smaller at higher concentrations. Data from Leighton & Acrivos (1987*b*) and Phan & Leighton (1996). Note that the solid line which provides a reasonable fit to the data is actually the best-fit formula found by Leighton & Acrivos (1986) for the effective diffusivity parallel to the plane of shear.

the shear-induced tracer diffusivity (or self-diffusivity for monodisperse suspensions) and is described by the coefficient $\hat{D}_\perp^{tr}$.

It is important to recognize that, as in the case of concentrated Brownian suspensions, the tracer diffusivity is very different from the collective or effective diffusivity $\hat{D}_\perp$. In concentrated systems, the effective diffusivity is dominated by the collective motion of particles down concentration gradients, and it is not necessary for particles to move past near neighbours for this collective motion to occur. In contrast, the random walk motion leading to the tracer diffusivity requires particles to exchange positions, a motion which is hindered at high concentrations. As a consequence, the effective diffusivity is much greater than the tracer diffusivity at high concentrations. This is illustrated in figure 3 in which the effective diffusivity normal to the plane of shear $\hat{D}_\perp$ (Leighton & Acrivos 1987*b*) and the tracer diffusivity normal to the plane of shear $\hat{D}_\perp^{tr}$ for $a_t/a_s = 1$ (Phan & Leighton 1996) are plotted. The effective diffusivity exceeds the tracer diffusivity by more than an order of magnitude at a suspension concentration of 45%.

Substituting equation (3) into equation (5) and rearranging, we obtain the tracer flux for $a_t/a_s = 1$:

$$(N_r)_t|_{a_t/a_s=1} = K_{r_\perp}\frac{\dot{\gamma}a_s^2}{r}\phi_s\phi_t - K_{\sigma_\perp}a_s^2\phi_s\phi_t\frac{\partial\dot{\gamma}}{\partial r} - \hat{D}_\perp^{tr}\dot{\gamma}a_s^2\frac{\partial\phi_t}{\partial r} - \left(\hat{D}_\perp - \hat{D}_\perp^{tr}\right)\dot{\gamma}a_s^2\frac{\phi_t}{\phi_s}\frac{\partial\phi_s}{\partial r} \quad (6)$$

in which the tracer flux is due to the curvature and shear gradient terms, and also due to both gradients in tracer concentration and the underlying suspension concentration. We may now extend this expression to tracers where $a_t/a_s \neq 1$ as

$$(N_r)_t = \beta_{r_\perp}\frac{\dot{\gamma}a_s^2}{r}\phi_s\phi_t - \beta_{\sigma_\perp}a_s^2\phi_s\phi_t\frac{\partial\dot{\gamma}}{\partial r} - \hat{D}_\perp^{tr}\dot{\gamma}a_s^2\frac{\partial\phi_t}{\partial r} - \delta_\perp\left(\hat{D}_\perp - \hat{D}_\perp^{sd}\right)\dot{\gamma}a_s^2\frac{\phi_t}{\phi_s}\frac{\partial\phi_s}{\partial r}. \quad (7)$$

The migration of tracers due to curvature is characterized by the coefficient $\beta_{r_\perp}$, by analogy with $K_{r_\perp}$. We anticipate that this will be a weak function of the suspension

concentration ϕ_s, and will equal $K_{r_\perp}$ in the limit $a_t/a_s = 1$. Likewise, the migration of tracers due to gradients in shear rate is characterized by $\beta_{\sigma_\perp}$, which again should equal $K_{\sigma_\perp}$ for $a_t/a_s = 1$. The effective diffusivity – the flux of tracers due to gradients in ϕ_s – must also be modified. We take this term to be given by $\delta_\perp \left(\hat{D}_\perp - \hat{D}_\perp^{sd}\right)$ where $\delta_\perp$ is expected to be a weak function of concentration, and to equal unity when $a_t/a_s = 1$. Here $\hat{D}_\perp^{sd}$ is the self-diffusion coefficient for a monodisperse suspension, e.g. the tracer diffusivity when $a_t = a_s$. The tracer diffusivity normal to the plane of shear $\hat{D}_\perp^{tr}$ has already been measured as a function of both concentration and tracer particle size (Phan & Leighton 1996).

In applying this model to parallel-plate flow we make two key simplifications. First, we recognize that the gradient in curvature and shear rate have the same radial dependence, thus

$$(N_r)_t = \beta \frac{\dot{\gamma} a_s^2}{r} \phi_s \phi_t - \hat{D}_\perp^{tr} \dot{\gamma} a_s^2 \frac{\partial \phi_t}{\partial r} - \delta_\perp \left(\hat{D}_\perp - \hat{D}_\perp^{sd}\right) \dot{\gamma} a_s^2 \frac{\phi_t}{\phi_s} \frac{\partial \phi_s}{\partial r} \tag{8}$$

where $\beta = \beta_{r_\perp} - \beta_{\sigma_\perp}$. Second, we make use of the experimental observations by Chapman (1990) and Chow *et al.* (1994) that the steady concentration profile $\phi_s(r)$ achieved for monodisperse suspensions is nearly uniform. This eliminates the last term in equation (8), leaving

$$(N_r)_t = \beta a_s^2 \phi_s \phi_t \frac{\dot{\gamma}}{r} - \hat{D}_\perp^{tr} \dot{\gamma} a_s^2 \frac{\partial \phi_t}{\partial r}. \tag{9}$$

The flux of tracer particles is thus characterized by just two terms: the difference between the curvature and shear gradient migration β and the tracer diffusivity. Since the latter of these two quantities has been measured, the focus of our work is to characterize β or the corresponding dimensionless radial tracer drift velocity $U_{tr}^* = \beta \phi_s$ as a function of a_t/a_s.

To analyse the time-dependent concentration distribution of tracer particles, we use the conservation equation

$$\frac{\partial \phi_t}{\partial t} = -\frac{1}{r} \frac{\partial (r(N_r)_t)}{\partial r}. \tag{10}$$

If we render r and t dimensionless by taking $r^* = r/R$ and $t^* = t/t_c$ where R is the radius of the upper plate and t_c is a characteristic time given by

$$t_c = \frac{R^2}{\hat{D}_\perp^{tr} (\Omega R/h) a_s^2} \tag{11}$$

and drop the asterisks, the dimensionless conservation equation becomes

$$\frac{\partial \phi_t}{\partial t} = \frac{-1}{r} \frac{\partial}{\partial r} \left\{ r \left[\frac{\beta \phi_s}{\hat{D}_\perp^{tr}} \phi_t - r \frac{\partial \phi_t}{\partial r} \right] \right\}. \tag{12}$$

Also, if we define

$$\alpha = \left(\frac{\beta \phi_s}{\hat{D}_\perp^{tr}} \right) \tag{13}$$

equation (12) reduces to

$$\frac{\partial \phi_t}{\partial t} = \frac{-1}{r} \frac{\partial}{\partial r} \left\{ r \left[\alpha \phi_t - r \frac{\partial \phi_t}{\partial r} \right] \right\}. \tag{14}$$

Note that while α will be a function of the size ratio a_t/a_s and the suspending sphere concentration ϕ_s, it should be independent of both position and time owing to the homogeneity of the suspending sphere concentration distribution. At steady state, the concentration profile ϕ_{t_∞} of the tracers is given by

$$\alpha\phi_{t_\infty} - r\frac{\partial\phi_{t_\infty}}{\partial r} = 0 \tag{15}$$

which gives

$$\phi_{t_\infty} = \tfrac{1}{2}(\alpha+2)\,\bar{\phi}_t r^\alpha \tag{16}$$

where the constant is determined from the conservation equation

$$\int_0^1 2\phi_{t_\infty} r\,\mathrm{d}r = \bar{\phi}_t. \tag{17}$$

To solve for the time-dependent concentration profile we let

$$\phi_t = \phi_{t_\infty} + \phi_d \tag{18}$$

where the governing equation for ϕ_d is given by

$$\frac{\partial\phi_d}{\partial t} = \frac{-1}{r}\frac{\partial}{\partial r}\left\{r\left[\alpha\phi_d - r\frac{\partial\phi_d}{\partial r}\right]\right\} \tag{19}$$

with the no-flux boundary conditions at $r = 0$ and $r = 1$

$$\left(\alpha\phi_d - r\frac{\partial\phi_d}{\partial r}\right)\Big|_{r=0,1} = 0 \tag{20}$$

and the initial condition

$$\phi_d|_{t=0} = \bar{\phi}_t - \phi_{t_\infty} = \bar{\phi}_t\left[1 - \tfrac{1}{2}(\alpha+2)\,r^\alpha\right]. \tag{21}$$

Now, if we attempt a separation of variables in r and t of the form

$$\phi_d = r^\alpha F(r)G(t) \tag{22}$$

we get for $G(t)$

$$G = \mathrm{e}^{-\sigma^2 t} \tag{23}$$

and correspondingly for $F(r)$ we get the eigenvalue problem

$$\left(r^{\alpha+2}F'\right)' + \sigma^2 r^\alpha F = 0 \tag{24}$$

such that $r^\alpha F'(r)|_{r=0,1} = 0$. The eigenfunctions F_n that satisfy the above equation are

$$F_n = r^{-(\alpha+1)/2} J_{\alpha+1}\left(2\sigma_n r^{1/2}\right) \tag{25}$$

which gives for the complete solution ϕ_t :

$$\phi_t(r,t) = \tfrac{1}{2}(\alpha+2)\,\bar{\phi}_t r^\alpha + \sum_{n=1}^{\infty} C_n F_n r^\alpha \mathrm{e}^{-\sigma_n^2 t}. \tag{26}$$

Here the eigenvalues σ_n and the coefficients C_n are obtained from the boundary condition at $r = 1$ and the initial condition respectively which gives for σ_n

$$J_{\alpha+2}(2\sigma_n) = 0 \tag{27}$$

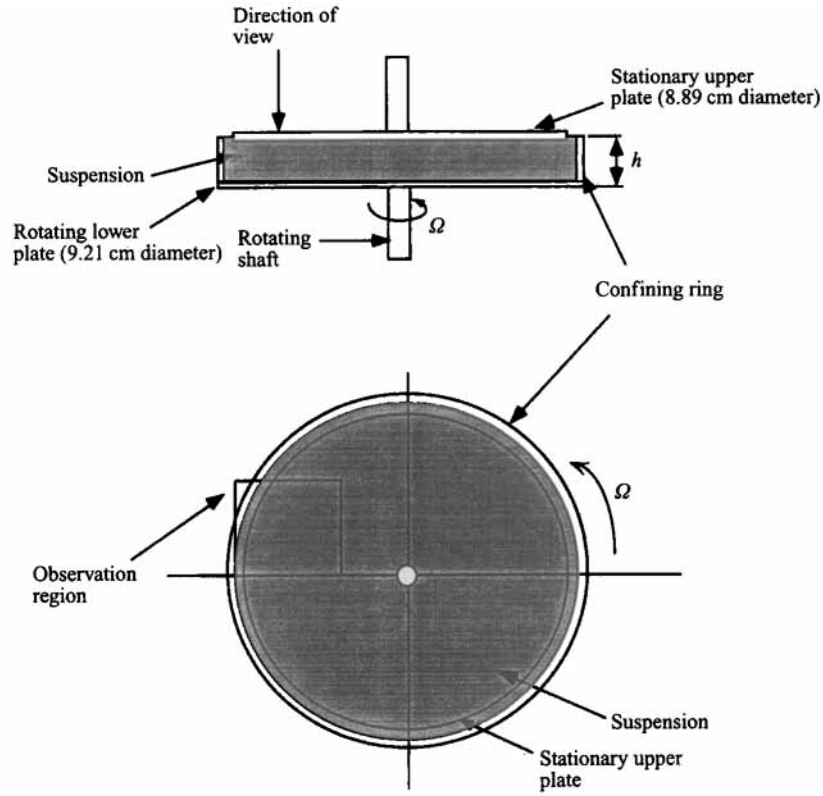

FIGURE 4. Experimental apparatus: parallel-plate device. The figure also shows top view of the device indicating the observation region. This rectangular region is divided into concentric bins of equal width but different area.

and for C_n

$$C_n = \frac{\int_0^1 \bar{\phi}_t \left[1 - \frac{1}{2}(\alpha+2) r^{\alpha}\right] r^{(1-\alpha)/2} J_{\alpha+1}\left(2\sigma_n r^{1/2}\right) \mathrm{d}r}{\int_0^1 J_{\alpha+1}^2\left(2\sigma_n r^{1/2}\right) \mathrm{d}r}. \tag{28}$$

We shall use these equations for the concentration distribution in analysing our results.

3. Experimental method

The experimental setup used was a parallel-plate viscometer (see figure 4). This consisted of a stationary upper plate and a rotating lower plate, both of which were made of PMMA to facilitate viewing the suspension. The radius of the upper plate was measured to be 8.89 cm and that of the lower plate was 9.21 cm. The solids used in our experiments were made of MG-102 PMMA obtained from ICI. The polydisperse material was sieved to obtain uniform fractions in the size ranges 425–500, 500–600 and 600–710 μm with an average density of 1.172 g cm^{-3}. The

average size of these fractions was determined optically to be $462 \pm 33, 539 \pm 59$ and 664 ± 73 μm respectively where the uncertainty is one standard deviation in the population size distribution rather than the error in the mean. A 45% (by volume) suspension of these particles was made using a mixture of 77.93% Triton X-100, 13.06% water, and 9.01% anhydrous zinc chloride which matched the refractive index and density of the acrylic particles. The pure suspending fluid had a viscosity of 37 p at the operating temperature of 27°C. The resulting suspension had a relative viscosity of about 17 and was loaded onto the parallel-plate device described above. The suspension was confined on the lower plate by means of an acrylic ring fitted around it.

Tracer particles of different sizes were used in our experiments. These particles were prepared by dyeing acrylic spheres with RIT liquid fabric dye. While most of the tracers were carefully selected from the same batch as the acrylic particles constituting the bulk suspension, the 1587 μm and 3175 μm tracer particles were ground acrylic spheres obtained from Engineering Laboratories, Inc. These particles were placed at different radial positions in the suspension near the centre of the lower plate. Once all the air bubbles that were entrained in the suspension during the mixing process had been removed, the upper plate was lowered so as to make uniform contact with the suspension, resulting in gap widths ranging between 0.7 and 1.0 cm. Once again, care was taken to exclude any air bubbles that might be trapped in the process. The suspension was sheared at shear rates varying from 1.18 to 4.96 s^{-1} (measured at the outer edge of the upper, stationary plate) and for dimensionless times $\hat{t}(\equiv \Omega a_s^2 t/Rh = t^*/\hat{D}_\perp^{tr})$ of about 0.6, where Ω is the angular velocity of the lower plate, a_s is the average radius of the suspending spheres, R is the radius of the upper plate and h the gap height.

The motion of the tracer particles was observed by viewing a small window of the suspension through the upper plate. For this purpose, a 45° front-surface mirror obtained from Melles Griot was used to record the images through a CCD colour camera. The resulting images were recorded on regular VHS tape using a Panasonic AG7500-A VCR. Care was taken to ensure that the mirror, the plates and the camera were all level for purposes of calibration and subsequent analysis. Owing to a limited field of vision, the exact centre of the device was outside the observation window. To determine the centre indirectly, a thread stretched radially outward over the upper plate from the central shaft was used. By digitizing a few points on the thread and knowing the exact radius of the upper plate, the coordinates of the centre of the device were determined.

For each of the larger tracer particles ($a_t/a_s > 2.0$), one single coloured tracer was placed at some radial position in the suspension. Once the shearing began, sufficient time was allowed to elapse such that any local concentration inhomogeneities present initially as a result of the loading procedure disappeared. The time necessary for this to occur scales with the shear-induced effective diffusivity $\hat{D}_\perp$ and occurs over a much faster time scale than the one governing the radial motion of the tracer particle. From the recorded images of an experiment, different frames were digitized to determine the radial position of the tracer every time that it completed one transit around the device.

As the ratio a_t/a_s was decreased below 2.0 the ratio of the random walk component to the drift velocity correspondingly increased, resulting in a larger relative error in the measurement of the migration velocities. Therefore the experiments with these smaller tracer particles were not analysed in the manner described above. For $a_t/a_s < 2.0$, a dilute concentration of the tracer particles (usually about 0.5 g of tracers in 250 g

of the total suspension) was added to the bulk suspension, stirred well to ensure a uniform distribution and then loaded onto the parallel-plate device. As before, all the entrained air bubbles were allowed to escape and the motion of the tracer particles was recorded on VHS tape for subsequent analysis.

The analysis procedure for these experiments involved digitizing many sets of frames using a Data Translation digitizing board on a 486DX. A typical image that is obtained is shown in figure 8. The observation region in each frame is divided into a number of radial bins of equal width but different areal coverage. Typically, the width of each bin was set at about 5–6 tracer particle diameters. The frames in each set were separated by a time interval sufficiently great so as to ensure statistical independence (typically on the order of 20 or so).

These frames were then temporally averaged to obtain a concentration profile that is representative of the particle distribution at average time of observation. Since the averaging occurred over a time scale of about 10 min, and the experiment took place over a time scale of many hours, no significant information is lost in the averaging process.

The number of frames chosen for the averaging process depended on the number density of the particles in each experiment. The exact number was chosen such that a total of at least 100 particle identifications were made in each bin giving a relative standard deviation of less than 10%. Each digitized frame was processed through a particle identification algorithm which determined the locations of the centres of the tracer particles. The algorithm essentially involved scanning each pixel location of the 512×512 image from left to right and top to bottom. The search concentrated on some prespecified region of the image that contained the particles and selected a low-intensity pixel (black), called 0 pixel, provided it was below a certain threshold value. Once a 0 pixel was found, four pixels in its neighbourhood were searched, one to its left and the three closest in the lower row, for the presence of 0 pixels. If 0 pixels were found in any or all of these four locations, they were connected together to form parts of a single particle.

In regions of high concentrations of the tracer particles it was observed that particles that were at about the same radial location, but at different vertical positions in the gap, tended to overlap with each other in the 2-D image. Under such a circumstance, the algorithm described above connects the overlapping particles counting them as a single entity. In order to minimize the effect of overlapping on the measured concentration distribution, a threshold limit was set on the size of the connected region in an image that was identified as a particle. If the 'particle' size was greater than 20 pixels, then it was counted as multiple particles at the same radial location.

4. Results

In general, the motion of the tracer particles was observed to be a combination of a steady drift and a random walk motion due to the random interactions of the tracers with other particles in the suspension. The motion of all the tracer particles investigated is reproduced in figure 5(*a–d*). Here, the tracer velocity is non-dimensionalized with respect to $\Omega a_s^2/h$, r with respect to R and t with respect to $Rh/\Omega a_s^2$. Note that the non-dimensional time $\hat{t}$ used in the analysis of these experiments is different from the t^* defined in equation (11), which is more appropriate for the concentration profile evolution experiments considered later on in this paper. The two quantities are related as $t^* = \hat{t}\hat{D}_\perp^{rr}$.

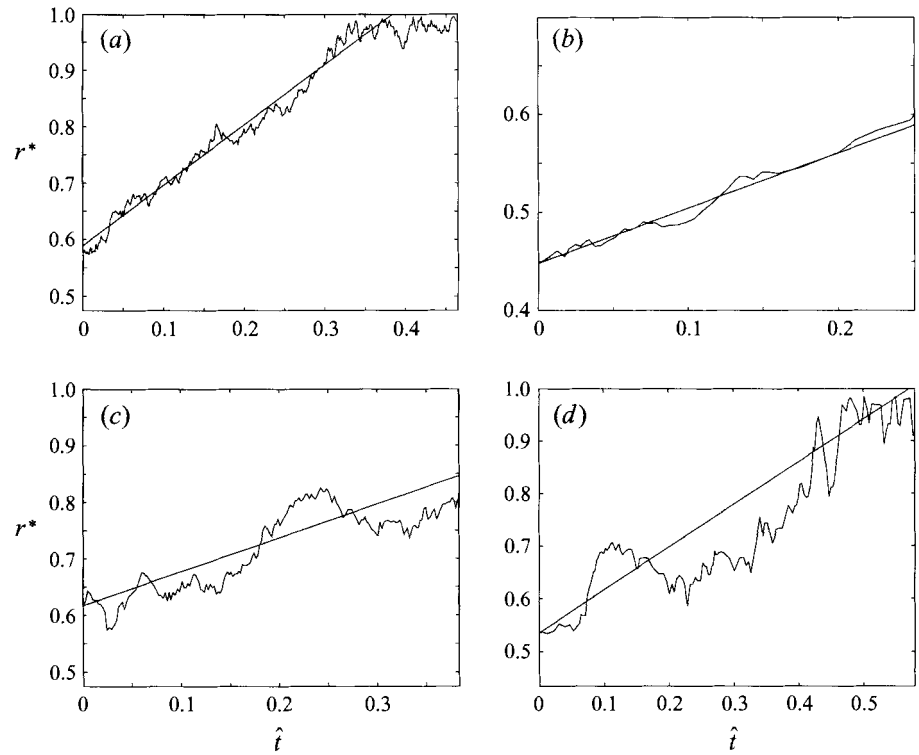

FIGURE 5. (*a*) Radial motion of a 3175 μm particle in a 45% suspension of 664 μm spheres. $U_{tr}^{*} = 1.071$ and $\hat{D}_{\perp}^{tr} = 0.015$. Here U_{tr}^{*} has been non-dimensionalized with respect to $\Omega a_s^2/h$, r^* with respect to R and $\hat{t}$ by $hR/\Omega a_s^2$. $\dot{\gamma} = 2.119\ \text{s}^{-1}$ at the outer edge, gap width = 1.0 cm, $a_t/a_s = 4.782$. (*b*) As (*a*) but for a 1587 μm particle in a 45% suspension of 462 μm spheres. $U_{tr}^{*} = 0.564$ and $\hat{D}_{\perp}^{tr} = 0.020$. $\dot{\gamma} = 1.990\ \text{s}^{-1}$ at the outer edge, gap width = 0.84 cm, $a_t/a_s = 3.435$. (*c*) As (*a*) but for a 1400 μm particle in a 45% suspension of 664 μm spheres. $U_{tr}^{*} = 0.599$ and $\hat{D}_{\perp}^{tr} = 0.030$. $\dot{\gamma} = 2.985\ \text{s}^{-1}$ at the outer edge, gap width = 0.71 cm, $a_t/a_s = 2.108$. (*d*) As (*a*) but for a 816 μm particle in a 45% suspension of 664 μm spheres. $U_{tr}^{*} = 0.811$ and $\hat{D}_{\perp}^{tr}$=0.052. $\dot{\gamma} = 4.199\text{s}^{-1}$ at the outer edge, gap width = 0.8 cm, $a_t/a_s = 1.229$.

As may be clearly seen, the outward drift velocity is approximately constant (independent of radial position), although the random walk can lead to a transient displacement inwards between successive observations. We can use such observations to calculate both the random walk tracer diffusivity and the average drift velocity. In the case of the 816 μm diameter tracer particle, the random walk was so large that it may have significantly influenced the calculated drift velocity. The tracer diffusivity is expected to be proportional to both the shear rate (which is, in turn, a function of position) and the suspension particle size (Leighton & Acrivos 1987*a*). For a constant observed drift velocity, we may calculate the tracer diffusivity as

$$\hat{D}_{\perp}^{tr} \equiv \frac{1}{2(N-1)} \sum_{i=1}^{N} \frac{(\Delta r_i - U_{tr}\Delta t_i)^2}{\Delta t_i \left(\Omega r_i/h\right) a_s^2} \tag{29}$$

where Δr_i is the radial displacement observed during time step Δt_i and r_i is the average radial position during this time step. The statistical error in this diffusivity arising from the random nature of the particle trajectory is described by the χ^2 distribution

and, for a large number of observations N, can be approximated by

$$\sigma_D \approx \hat{D}_{\perp}^{tr}(2/N)^{1/2}. \tag{30}$$

The average drift velocity is also calculated from the observed motion of the particle. One way of calculating this is by simply taking the beginning and end points of the migration and dividing by the elapsed time. A more accurate approach, however, is to take each individual observed displacement, calculate a velocity, and take a weighted average of them. The weighting function is the variance in each calculated velocity due to the time between observations and the random walk tracer diffusivity at that radial position. If the diffusivity is constant, the two approaches to calculating the drift velocity are identical. For the parallel-plate geometry, however, the tracer diffusivity is proportional to the shear rate and hence increases with radial position away from the centre. Therefore, the weighting function used in our calculations is given by

$$1/\sigma_i^2 \equiv \frac{\Delta t_i}{2\hat{D}_{\perp}^{tr}(\Omega r_i/h)a_s^2} \tag{31}$$

which, in effect, preferentially weights the observations at smaller radial positions or with a smaller random walk. Thus, the appropriately weighted drift velocity is given by

$$U_{tr} = \sum_{i=1}^{N} \Delta r_i/r_i \Bigg/ \sum_{i=1}^{N} \Delta t_i/r_i. \tag{32}$$

The drift velocity calculated using the above equation differs only slightly from that calculated using the end points of the migration. The error in the calculated drift velocity is given approximately by

$$\sigma_U^2 \approx \frac{2\hat{D}_{\perp}^{tr}\left(\Omega\langle r_i\rangle/h\right)a_s^2}{\sum_{i=1}^{N}\Delta t_i} \tag{33}$$

where $\langle r_i\rangle$ is the average radial location of the tracer particle.

In the calculation of the drift velocities and diffusivities, care was taken to ensure that only particle motions that began more than $4\sigma_U + h$ away from the outer edge of the upper plate were considered. This was done to avoid any influence of the wall on the calculated velocities. Further improvement in statistical accuracy was obtained by summing successive jumps of the random-walk motion, analogous to the approach used by Leighton & Acrivos (1987*a*). Table 1 gives the random-walk diffusivities, drift velocities, and the associated errors for the individual tracer particles investigated. Each of the values given in the table is averaged over different runs. Note that the errors shown in the table do not include any observational errors such as those due to the camera and the plates not being exactly parallel. A piece of graph paper attached to the stationary plate was used to determine the angle made between the camera and the vertical which was then used to correct for any misalignment. Therefore, such fixed errors were presumed to be negligible.

The variance in the drift velocities in the table is calculated as a weighted average of the mean-square deviations of the drift velocities for N different runs and a particular

$2a_t(\mu m)$	$2a_s(\mu m)$	a_t/a_s	$\langle U^*_{tr}\rangle$	$\sigma_{U^*_{tr}}$	$\hat{D}^{tr}_{\perp}$	$\sigma_{\hat{D}^{tr}_{\perp}}$	h(cm)	$\dot{\gamma}(s^{-1})$
3175	664	4.782	1.134	0.0518	0.016	0.0023	1.00	2.119
1587†	462	3.435	0.564	—	0.020	0.0100	0.84	1.990
1400	664	2.108	0.362	0.0783	0.035	0.0041	0.71	2.985
816	664	1.229	0.498	0.1569	0.039	0.0067	0.80	4.199

TABLE 1. Calculated dimensionless drift velocities and the corresponding tracer diffusivities for the different experiments together with the standard deviations.
† Involves data from one run only.

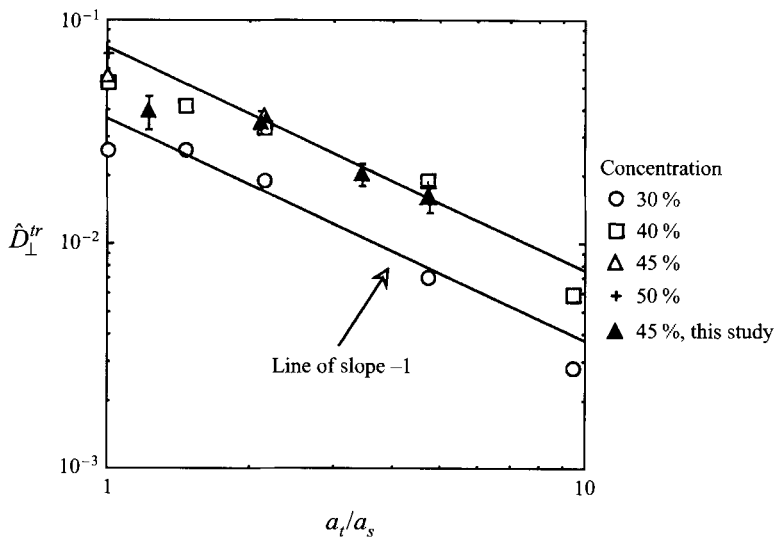

FIGURE 6. Comparison of tracer diffusivity measurements made in this work with those of Phan & Leighton (1996). For $a_t/a_s \geqslant 2.0$, Phan & Leighton found $\hat{D}^{tr}_{\perp}$ to vary approximately as $0.079a_t/a_s$.

value of the ratio a_t/a_s:

$$\sigma_{U^*_{tr}} = \left(\frac{1}{N} \frac{\sum_{i=1}^{N} \left(U^*_{tr,i} - \langle U^*_{tr}\rangle^2\right) t^*_i}{\sum_{i=1}^{N} t^*_i} \right)^{1/2}. \tag{34}$$

Here, $U^*_{tr,i}$ is the tracer velocity for an individual run and $\langle U^*_{tr}\rangle$ the average over different runs. From the data, it is clear that as the ratio of the tracer particle radius to the suspending sphere radius (a_t/a_s) was decreased, the magnitude of the random-walk drift increased and became significant relative to the magnitude of the steady outward drift velocity itself. In fact, such an observation is consistent with those of Phan & Leighton (1996), who found that the tracer diffusivity normal to the plane of shear in a Couette device varied as approximately $0.079a_s/a_t$ for $a_t/a_s \geqslant 2$ and suspension concentrations between 40% and 50% by volume (see figure 6).

For the smaller size ratios, the drift velocities were inferred indirectly from the concentration profile evolution experiments referred to in §3. The concentration

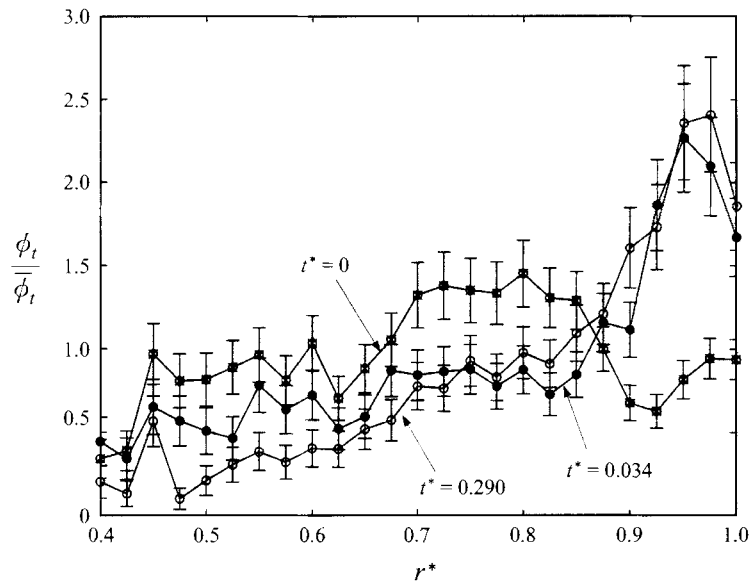

FIGURE 7. Concentration profile evolution of 816 μm tracer particles in a 45% concentration (by volume) suspension of 462 μm particles at $t^* = 0.0, 0.034$ and 0.290 with 1σ error bars. Notice the migration of the tracer particles towards the outer edge of the device with elapsed strain.

distribution of the tracers was obtained by counting the number of tracer particle observations in each bin and subsequently normalizing it with the area of the bin. The width of each bin typically being about 5–6 particle diameters across the error induced by the presence of a finite-sized bin on the distribution of the tracers was ignored. The number density of particles was then obtained by performing a temporal average over the different frames. The initially observed concentration profile and its subsequent evolution to its steady state is shown in figure 7 with 1σ error bars for the particular case of 816 μm tracer particles in a suspension of average diameter 462 μm. As can be seen, the initial profile is more or less uniform radially whereas the steady-state profile indicates that the tracer particles have migrated outward resulting in a higher concentration of the tracers near the outer edge of the device. Recall that a similar behaviour was also observed in the individual tracer particle experiments, where the motion of a single tracer particle was followed as a function of time. This can also be seen from figure 8 which shows the initial and final distribution of large tracer particles in a particular experiment. Once again, a higher density of particles near the outer edge of the device is indicative of the large tracers migrating towards regions of larger shear stress or lower curvature. In the experiments where the ratio a_t/a_s was less than 1 (i.e. the tracer particles were smaller than those constituting the bulk of the suspension), the tracer particles displayed a tendency to move radially inwards towards regions of higher curvature (or lower shear stress).

In order to obtain a quantitative comparison between these experimental observations and the theoretical description provided in §2, we examine the drift velocities of the tracer particles arising from the migration mechanism. The magnitude of these migration velocities can be obtained by comparing the steady-state concentration profile obtained in these experiments with the theoretically predicted steady-state concentration distribution (equation (16)). The advantage of using such a technique is that the accuracy of the measurements is independent of the random walk of the

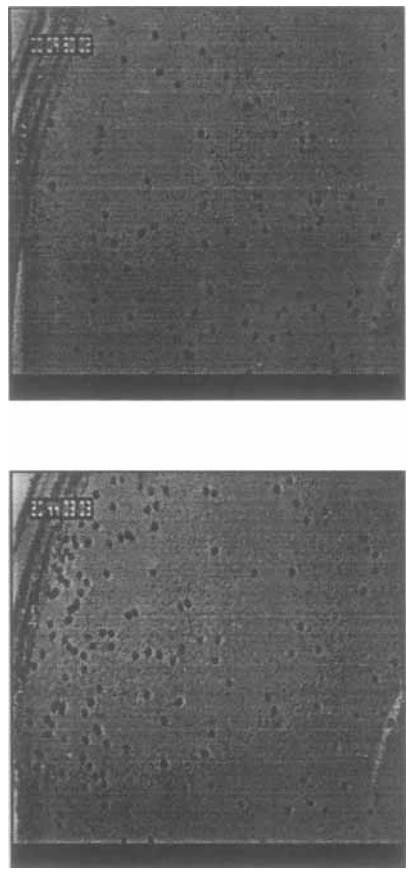

FIGURE 8. (*a*) Initial ($t^* = 0$) and (*b*) final ($t^* = 0.102$) concentration profiles of 944 μm tracer particles in a 45% concentration (by volume) suspension of 664 μm particles. The underlying bulk suspension appears grey and the tracer particles are coloured black in the above images. Notice the inhomogeneous concentration distribution of the tracer particles in the final state. The final state in the experiment, $t^* = 0.102$, corresponds to more than 20 hours of shearing.

tracer particles and is a function only of the accuracy of the particle identification procedure. Therefore, such a procedure enables us to determine the long-time behaviour without requiring the continuous tracking of the tracer particles over consecutive transits around the parallel-plate device. Figure 9(*a–e*) shows log-log plots of the final concentration profiles obtained in each of the runs together with the corresponding experimental conditions.

As can be seen from figure 9(*b*), for $a_t/a_s < 1$ the tracer particles exhibited a behaviour opposite to that of the larger tracer particles, which ultimately resulted in a higher concentration near the centre of the device. From equation (16) it is immediately obvious that fitting a straight line in the above figures yields the value of α for each experiment where the quantity α is related to the migration velocity of the tracer particles through the relation

$$U_{tr} = \beta a_s^2 \frac{\Omega}{h} \phi_s \equiv \frac{\alpha D_{tr}}{R} \tag{35}$$

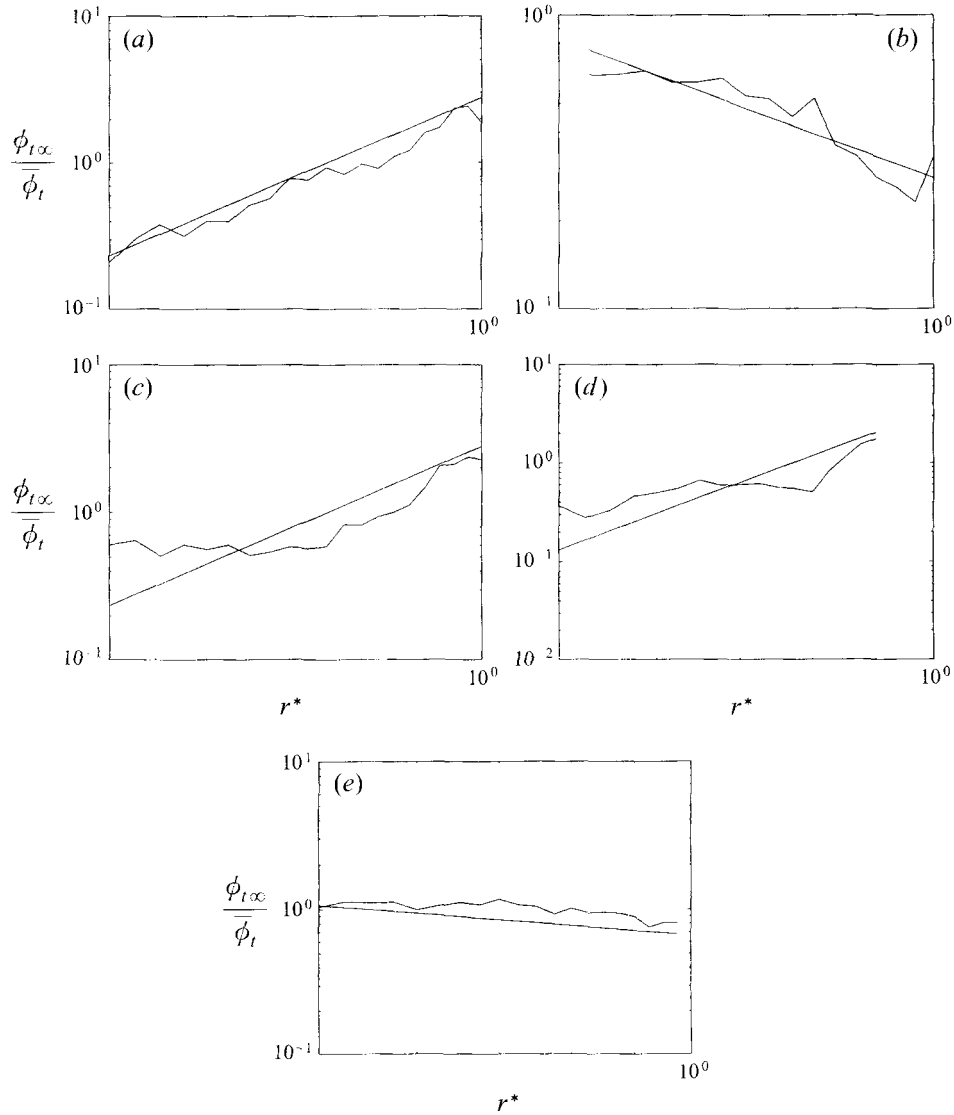

FIGURE 9. Final tracer concentration distribution in a suspension of overall concentration 45%. (*a*) $t^* = 0.290$, $\dot{\gamma} = 4.238\ \text{s}^{-1}$ at the outer edge, gap width = 0.787 cm, $2a_t = 816\ \mu\text{m}$, $2a_s = 462\ \mu\text{m}$, $a_t/a_s = 1.766$, $\alpha = 3.570$. (*b*) $t^* = 0.154$, $\dot{\gamma} = 2.144\ \text{s}^{-1}$ at the outer edge, gap width = 0.780 cm, $2a_t = 462\ \mu\text{m}$, $2a_s = 664\ \mu\text{m}$, $a_t/a_s = 0.696$, $\alpha = -2.138$. (*c*) $t^* = 0.102$, $\dot{\gamma} = 1.946\ \text{s}^{-1}$ at the outer edge, gap width = 0.86 cm, $2a_t = 944\ \mu\text{m}$, $2a_s = 664\ \mu\text{m}$, $a_t/a_s = 1.422$, $\alpha = 3.565$. (*d*) $t^* = 0.082$, $\dot{\gamma} = 1.995\ \text{s}^{-1}$ at the outer edge, gap width = 0.838 cm, $2a_t = 944\ \mu\text{m}$, $2a_s = 462\ \mu\text{m}$, $a_t/a_s = 2.043$, $\alpha = 4.651$. (*e*) $t^* = 0.302$, $\dot{\gamma} = 1.935\ \text{s}^{-1}$ at the outer edge, gap width = 0.864 cm, $2a_t = 462\ \mu\text{m}$, $2a_s = 539\ \mu\text{m}$, $a_t/a_s = 0.857$, $\alpha = -0.663$.

or

$$U_{tr}^* = \beta\phi_s \equiv \alpha\hat{D}_\perp^{tr} \tag{36}$$

and is given by the slope of the fitted line.

Having obtained the value of α, we can now look at the time-dependent concentration profile evolution predicted by equation (26). Figure 10 shows the theoretically calculated concentration profiles at different times for $a_t/a_s = 1.766$ and a value of

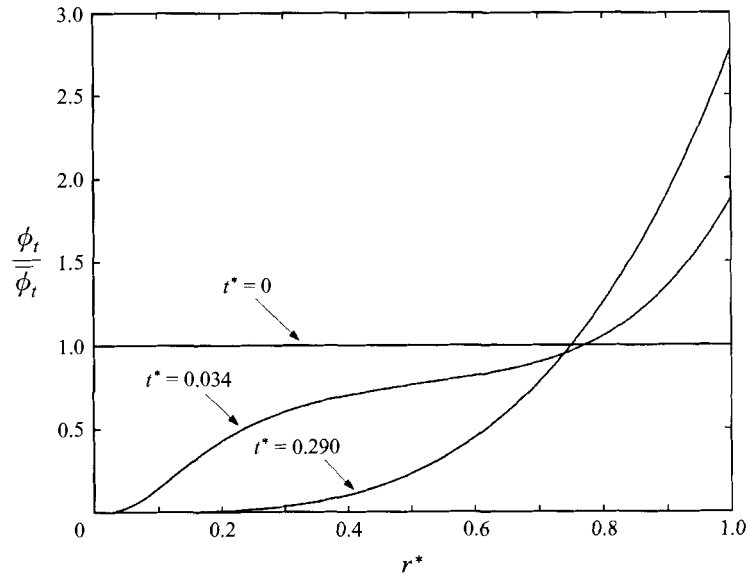

FIGURE 10. Theoretically calculated concentration profile evolution for $2a_t = 816$ μm, $2a_s = 462$ μm ($a_t/a_s = 1.766$). $\dot{\gamma} = 4.238\text{s}^{-1}$ at the outer edge, gap width = 0.787 cm and $\alpha = 3.57$.

$\alpha = 3.57$. As also observed from the experimental data under the same set of conditions (figure 7), the model predicts an initially homogeneous concentration profile and a subsequent relaxation to an inhomogeneous one as a function of elapsed strain. From this it appears that the theory provides at least a qualitative description of the migration process. Unfortunately, the large scatter in the experimental observations renders direct comparison of the experimental and theoretical profiles difficult.

In order to evaluate the transient results quantitatively, we use instead an integrated measure of the tracer particle positions. One such measure is the average radial position of the particles in the observation window given by

$$I(t^*) = \int_\epsilon^1 \phi_t r^{*2} \mathrm{d}r^* \Big/ \int_\epsilon^1 \phi_t r^* \mathrm{d}r^* \tag{37}$$

where $\epsilon < r^* < 1$ is the region of observation in an experiment. The inner limit of observations ϵ varied between 0.3 and 0.5 for different experiments. At steady state, this average radial position is solely a function of α. If we substitute the theoretically obtained steady-state concentration profile into equation (37), this limit becomes

$$I|_{t^*=\infty} = \left(\frac{\alpha+2}{\alpha+3}\right)\left[\frac{1-\epsilon^{\alpha+3}}{1-\epsilon^{\alpha+2}}\right]. \tag{38}$$

Thus, the steady average radial position is a measure of the ratio α of the migration velocity U_{tr}^* to the diffusivity $\hat{D}_\perp^{tr}$, and the rate with which it approaches steady state is governed by both α and the diffusivity.

Figure 11(*a–d*) shows plots of $I(t^*)$ versus t^* for the various size ratios investigated. Both the experimental and the corresponding theoretically calculated values of $I(t^*)$ are shown. Rather than simultaneously varying both α and $\hat{D}_\perp^{tr}$, the theoretical profiles for $I(t^*)$ were instead calculated by using the values for the diffusivity $\hat{D}_\perp^{tr}$ obtained from the independent measurements of Phan & Leighton (1996) and performing a one-parameter curve fit over α. The theoretical steady profiles depicted in figure 9

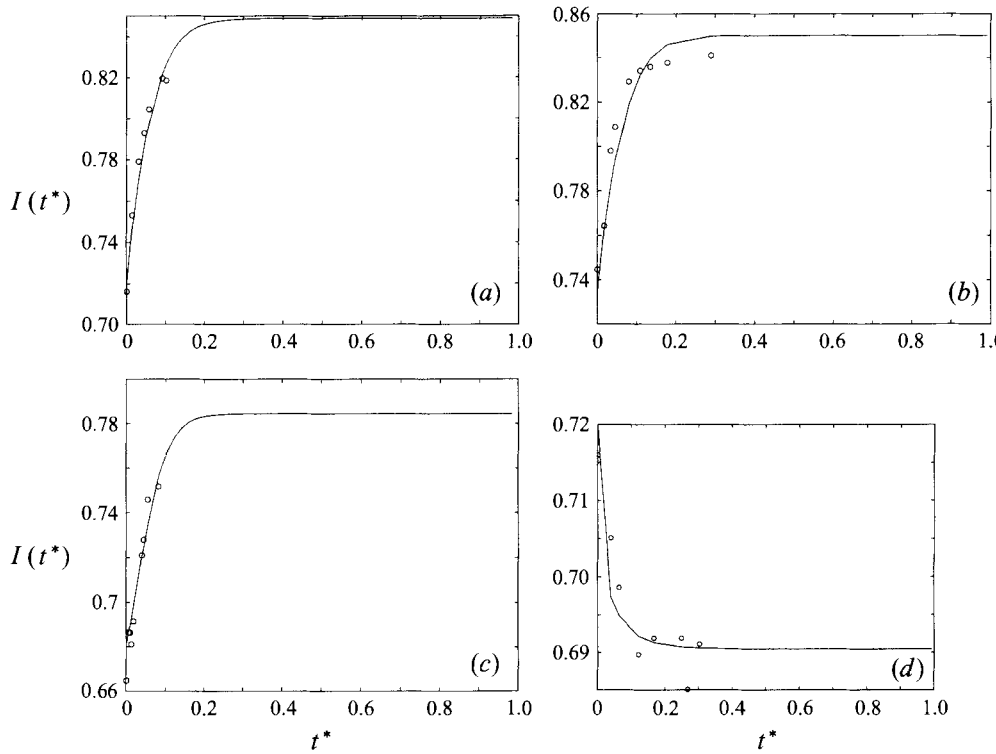

FIGURE 11. (*a*) $I(t^*)$ obtained from experimental observations as well as from the theoretical model for $2a_t = 944$ μm, $2a_s = 664$ μm ($a_t/a_s = 1.422$). The open circles are the experimental data. The solid line corresponds to the theoretically calculated value of I for an $\alpha = 3.565$ and $\hat{D}_\perp^{tr} = 0.0457$ (from Phan & Leighton 1996). $\epsilon = 0.325$, $\dot{\gamma} = 1.946\text{s}^{-1}$ at outer edge, gap width = 0.86 cm. (*b*) As (*a*) but for $2a_t = 816$ μm, $2a_s = 462$ μm ($a_t/a_s = 1.766$); $\alpha = 3.57$ and $\hat{D}_\perp^{tr} = 0.039$. $\epsilon = 0.375$, $\dot{\gamma} = 4.238$ s^{-1} at outer edge, gap width = 0.787 cm. (*c*) As (*a*) but for $2a_t = 944$ μm, $2a_s = 462$ μm ($a_t/a_s = 2.043$); $\alpha = 4.651$ and $\hat{D}_\perp^{tr} = 0.0351$. $\epsilon = 0.4$, $\dot{\gamma} = 1.995$ s^{-1} at outer edge, gap width = 0.838 cm. (*d*) As (*a*) but for $2a_t = 462$ μm, $2a_s = 539$ μm ($a_t/a_s = 0.857$); $\alpha = -0.663$ and $\hat{D}_\perp^{tr} = 0.056$. $\epsilon = 0.375$, $\dot{\gamma} = 1.935$ s^{-1} at outer edge, gap width = 0.864 cm.

were also calculated in this manner. As can be seen, in most cases a reasonable fit is obtained between the experimental data and the theoretical calculations. Figure 11(*b*) for the case of $2a_t = 816$ μm and $2a_s = 462$ μm however, shows that the best fit value of α that is obtained overpredicts the steady-state value of $I(t^*)$. The values of $\hat{D}_\perp^{tr}$ and α used to obtain this curve are 0.039 and 3.57 respectively. If, instead, we perform a two-parameter fit and use values of $\hat{D}_\perp^{tr} = 0.062$ and $\alpha = 3.16$, then we obtain an exact fit between theory and experiment, as one might expect. While it is clear that the rate at which the steady profile is approached is at least qualitatively consistent with a migration process governed by the shear-induced tracer diffusivity, it remains to explain this discrepancy.

For two of the size ratios studied (figures 11*a* and 11*c*) we did not reach the steady-state concentration profile despite over 20 hours of shearing. A value of α and hence U_{tr} can still be determined, however, as outlined above. Notice that figure 11(*d*) shows the concentration profile variation for a case where $a_t/a_s < 1$. In this case, as mentioned earlier, it turns out that the tracer particles tend to move radially inwards rather than outwards, as observed for $a_t/a_s > 1$.

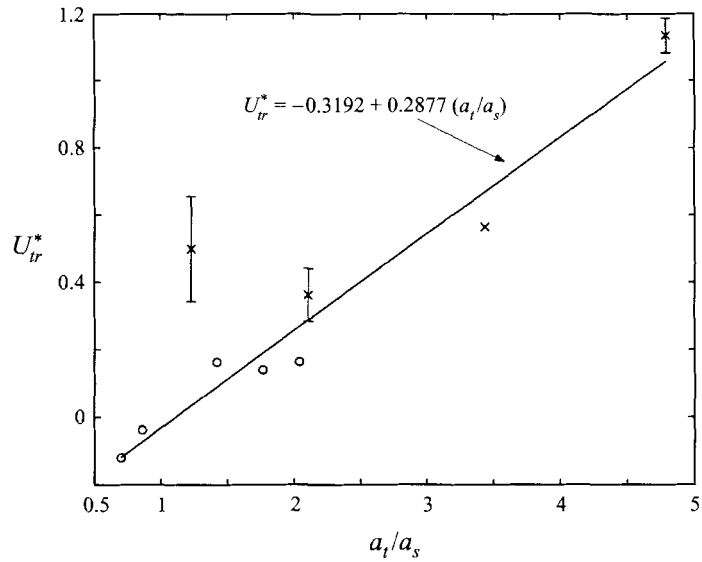

FIGURE 12. Combined results from the tracer particle (×) and concentration profile evolution (○) experiments. Note that the data for $2a_t = 1587$ μm and $2a_s = 462$ μm ($a_t/a_s = 3.435$) involve only a single experimental run. The drift velocity of tracer particles shows a roughly linear behaviour and a value of about zero when $a_t = a_s$, i.e. when the suspension is monodisperse. Error bars are one standard deviation obtained from statistical sources.

We may now combine the results obtained from the individual tracer particle measurements as well as the concentration profile evolution experiments to determine the migration velocity of tracer particles in a monodisperse suspension as a function of the ratio a_t/a_s. Since this drift velocity is related to the function $\beta(a_t/a_s)$ we can simultaneously determine the correction to the particle fluxes for monodisperse suspensions induced by gradients in shear rate and curvature as a function of a_t/a_s (figure 12). For the individual tracer particle experiments β is calculated from $U_{tr}^*/\phi_s \equiv U_{tr}h/(\Omega a_s^2\phi_s)$. For the concentration profile measurements this is determined by $\beta = \alpha\hat{D}_\perp^{tr}/\phi_s$ (equation (36)) where we use the tracer diffusivities measured by Phan & Leighton to calculate the drift velocity from the steady concentration profile. The data from the concentration profile evolution experiments are shown in table 2. The drift velocity data of the tracer particles from both kinds of experiments exhibit a similar variation with a_t/a_s and show a roughly linear increase with this ratio. Note that in figure 12 we have rendered the velocity dimensionless with the scaling appropriate for shear-induced migration. Making a linear fit to the data, for the case of a_t equal to a_s, it appears that the drift velocity is close to zero (within experimental error) when the suspension consists of particles of one size only. This is in agreement with the observations of Chow *et al.* (1994) and Chapman (1990) discussed earlier.

5. Discussion

The only previous previous investigation involving shear-induced migration of bidisperse suspensions in curved geometries was that of Abbott *et al.* (1991) in a wide-gap Couette device. In that study it was observed that larger particles migrated outward to regions of lower shear rate (or shear stress). They ascribed this behaviour to a drift induced by gradients in shear rate. In our experiments with tracer particles,

$2a_i(\mu m)$	$2a_s(\mu m)$	a_i/a_s	α	U_{tr}^*	$\hat{D}_\perp^{rr}$†	h(cm)	$\dot{\gamma}(s^{-1})$
816	462	1.766	3.570	0.139	0.039	0.79	4.238
462	664	0.696	−2.138	−0.120	0.056	0.78	2.144
944	664	1.422	3.565	0.164	0.046	0.86	1.946
944	462	2.043	4.651	0.163	0.035	0.84	1.995
462	539	0.857	−0.663	−0.037	0.056	0.86	1.935

TABLE 2. Results from the concentration profile evolution experiments.
† Data from Phan & Leighton (1996).

we observed a similar behaviour, in that tracer particles larger than those making up the suspension tended to migrate radially outward. In our experiments, however, the radially outward migration resulted in migration to regions of higher shear rate rather than lower. The discrepancy between these two experiments may be reconciled if we take into consideration the migration of particles due to the curvature in the geometry, as introduced in §2.

In order to understand this better, it is worthwhile to examine the local velocity distributions induced by the two rotational geometries: (*a*) parallel-plate flow and (*b*) wide-gap Couette flow. We shall focus on the velocity distribution in the vicinity of some point $y_i = R\delta_{i2}$. Because the streamlines of such a flow are circular, for simplicity we shall use a rotating reference frame such that the local velocity at this point is zero. Let us first consider the parallel-plate flow given by

$$u_i = \frac{\Omega}{h}(\delta_{i1}x_2 - \delta_{i2}x_1)\,x_3 \tag{39}$$

in which the axis of rotation is given by δ_{i3}. The local velocity in the vicinity of the point $y_i = R\delta_{i2}$ is given by

$$u_i = \frac{\Omega}{h}\left(\delta_{i1}Rx_3' + \delta_{i1}x_3'x_2' - \delta_{i2}x_3'x_1'\right) \tag{40}$$

where $x_i' = x_i - y_i$. The first term in this expression represents the local shear rate. The second term induces a gradient in this shear rate which, according to the model of Leighton & Acrivos (1987*b*) and Phillips *et al.* (1992) can lead to particle migration. In addition to these two terms, however, there is a third term which is the coupling of the velocity gradient with the curvature of the streamlines: the curvature of the streamlines decreases for any outward motion of a particle. If the gradient in shear rate caused by the second term produces an inward migration of larger tracer particles to regions of lower shear rate (as has been proposed in wide-gap Couette flow), this final term must more than offset this migration to lead to the observed net outward motion for large tracers.

In a similar fashion, we may make an expansion of the velocity distribution in wide-gap Couette flow about the same point yielding a similar local velocity profile:

$$u_i \approx C\left(\delta_{i1}Rx_2' - \delta_{i1}\tfrac{1}{2}\left(x_2'^2 - x_1'^2\right) - \delta_{i2}x_2'x_1'\right) \tag{41}$$

where we have truncated after quadratic terms. The constant C is given by $2\kappa^2R_0^2\Omega/[R^3(1-\kappa^2)]$. In this equation R_0 is the radius of the outer cylinder and κ is the ratio of the inner radius to R_0. The principal difference between this expression and that for parallel-plate flow is the sign of the shear-gradient term. For Couette flow the shear rate is reduced with increasing R, rather than increasing as in

parallel-plate flow. With the curvature term unchanged, the above analysis suggests that for this geometry both the curvature and shear-gradient terms lead to an outward radial migration of large tracer particles. Thus, in Couette flow it is difficult to separate the two effects. In the parallel-plate geometry on the other hand, the curvature-induced migration opposes that due to the gradient in shear stress and the two effects seem to cancel each other out for the case of monodisperse suspensions.

One possible explanation for our observations, other than the shear-induced migration model presented earlier, could be the presence of inertial effects such as radial secondary currents. These arise because of a finite Reynolds number (Re) and result in fluid being convected radially outward near the rotating plate and radially inward near the stationary plate. The velocity field to $O(Re)$ may be obtained as a regular perturbation expansion of the unidirectional base flow. The radial and vertical components of this velocity (v_r, v_z) are given by (Leighton 1985)

$$v_r = \frac{\rho\Omega^2 h^2}{60\mu} r \left(5z^{*4} - 9z^{*2} + 4z^*\right) \tag{42}$$

and

$$v_z = \frac{\rho\Omega^2 h^3}{30\mu} \left(-z^{*5} + 3z^{*3} - 2z^{*2}\right). \tag{43}$$

Here, ρ is the density of the fluid, r is the radial position away from the centre and z^* is the vertical distance within the gap non-dimensionalized with respect to the height h. A characteristic time (t_{sc}) necessary for these secondary currents to sweep particles outward or inward, may be taken as the time necessary for a particle to move across half the plate radius at the maximum radial velocity. This is therefore given by

$$t_{sc} \approx \frac{60\mu_r\mu_o R^2}{\rho\dot{\gamma}^2 h^4} \tag{44}$$

where μ_r and μ_o stand for the relative viscosity of the suspension and the viscosity of the suspending fluid respectively and the shear rate is measured at the outer edge of the plate. For typical values of the parameters of our system t_{sc} was calculated to be on the order of $\sim$ 200 hours or so at least, which is about a factor of 2 to 3 larger than the characteristic time taken by the tracers to reach their steady-state position. Note that equation (44) is based on the maximum radial velocity; in reality however, the particle has an equal probability of sampling all the velocity streamlines due to the random-walk motion in the vertical direction. As such, the actual relevant time scale over which secondary currents play a significant role is likely to be much larger. As a direct test to determine the relative importance of the radial secondary currents, the individual tracer particle experiments were carried out with two different suspending fluids: (*a*) Triton X-100 with a viscosity of 2.4 P and (*b*) a Triton X-100, zinc chloride, water solution with a viscosity of 37 P. In spite of an order of magnitude difference in the viscosity of the two fluids, the time taken for an individual tracer particle to migrate radially outward was found to be about the same. To further confirm the negligible effect of these radial secondary currents, the effect of shear rate on the migration phenomenon was also studied. It was found that when the shear rate was doubled, the time taken for a tracer particle to reach its steady-state position correspondingly decreased by a factor of around 2 rather than 4 as might be expected if secondary currents were the cause of the radial migration. Therefore, we may conclusively rule out the effect of radial secondary currents on the radial drift observed here.

As an extension of this work and that of Abbott *et al.*, another geometry of interest is cone-and-plate flow. In this geometry, since there is no radial variation in the shear rate, one would expect that only the curvature-induced migration would play any role and result in a net outward migration even for monodisperse suspensions.

This work was supported in part by Lockheed Missiles and Space Co., Inc.

REFERENCES

ABBOTT, J. R., TETLOW, N. GRAHAM, A. L. ALTOBELLI, S. A. FUKUSHIMA, E. MONDY, L. A. & STEPHENS, T. S. 1991 Experimental observations of particle migration in concentrated suspensions: Couette flow. *J. Rheol.* **5**, 773–795.

ARP, P. A. & MASON, S. G. 1977 Kinetics of flowing dispersions 9 – doublets of rigid spheres (experimental). *J. Colloid Interface Sci.* **61**, 44.

CHAPMAN, B. K. 1990 Shear induced migration phenomena in concentrated suspensions. PhD thesis, University of Notre Dame.

CHAPMAN, B. K. & LEIGHTON, D. T. 1991 Dynamic viscous resuspension. *Intl J. Multiphase Flow* **17**, 469–483.

CHOW, A. W., SINTON, S. W., IWAMIYA, J. H. & STEPHENS, T. S. 1994 Shear-induced migration in Couette and parallel-plate viscometers: NMR imaging and stress measurements. *Phys. Fluids* A **6**, 2561–2576.

KOH, C. J., HOOKHAM, P. & LEAL, L. G. 1994 An experimental investigation of concentrated suspension flows. *J. Fluid Mech.* **266**, 1–32.

LEIGHTON, D. T. 1985 The shear induced migration of particulates in concentrated suspensions. PhD thesis, Stanford University.

LEIGHTON, D. T. & ACRIVOS, A. 1986 Viscous resuspension. *Chem. Engng Sci.* **41**, 1377–1384.

LEIGHTON, D. T. & ACRIVOS, A. 1987*a* Measurement of shear-induced self-diffusion in concentrated suspensions of spheres. *J. Fluid Mech.* **177**, 109–131.

LEIGHTON, D. T. & ACRIVOS, A. 1987*b* The shear-induced migration of particles in concentrated suspensions. *J. Fluid Mech.* **181**, 415–439.

LEIGHTON, D. T. & RAMPALL, I. 1993 Measurement of the shear-induced microstructure of concentrated suspensions of non-colloidal particles. In *Particulate Two-Phase Flow* (ed. M. C. Roco). Butterworth.

NOTT, P. R. & BRADY, J. F. 1994 Pressure-driven flow of suspensions: simulation and theory. *J. Fluid Mech.* **275**, 157–199.

PHAN, S. & LEIGHTON, D. T. 1996 Measurement of the shear-induced tracer diffusivity in concentrated suspensions. *J. Fluid Mech.* (submitted).

PHILLIPS, R. J., ARMSTRONG, R. C., BROWN, R. A., GRAHAM, A. L. & ABBOTT, J. R. 1992 A constitutive equation for concentrated suspensions that accounts for shear-induced particle migration. *Phys. Fluids* A **4**, 30.

SCHAFLINGER, U., ACRIVOS, A. & ZHANG, K. 1990 Viscous resuspension of a sediment within a laminar and stratified flow. *Intl J. Multiphase Flow* **16**, 567–578.